Research Article | Vol. 8, No. 1 | 1 Jan 2017 | BIOMEDICAL OPTICS EXPRESS 230
Biomedical Optics EXPRESS

# Anti-confocal assessment of middle ear inflammation

DAVID S. JUNG,[1,2,*] JOHN A. CROWE,[2] JOHN P. BIRCHALL,[1,3] MICHAEL G. SOMEKH,[2,4] AND CHUNG W. SEE[2]

[1]*National Institute for Health Research (NIHR) Nottingham Hearing Biomedical Research Unit, 113 The Ropewalk, Nottingham, NG1 5DU, UK*
[2]*Department of Electrical and Electronic Engineering, University of Nottingham, University Park, Nottingham, NG7 2RD, UK*
[3]*Otology and Hearing group, Division of Clinical Neuroscience, School of Medicine, University of Nottingham, Nottingham, NG7 2UH, UK*
[4]*Department of Electronic and Information Engineering, The Hong Kong Polytechnic University, Hung Hom, Kowloon, Hong Kong, China*
[*]*david.jung@nottingham.ac.uk*

**Abstract:** To improve the diagnostic prediction of recurrence of otitis media with effusion after surgery, an anti-confocal system combined with spectroscopic measurements is proposed to reject unwanted signals from the eardrum and assess the blood content. The anti-confocal system was experimentally evaluated on both optical middle ear phantom and human skin. Results showed effective rejection of signals from the eardrum using a central stop replacing the confocal pinhole, while still detecting signals from the middle ear mucosa. The system is sensitive to changes in blood content, but scattering and absorption characteristics of the eardrum can distort the measurement. Confocal detection of eardrum properties was shown to be a promising approach to correct measurements.



**OCIS codes:** (170.1790) Confocal microscopy; (170.3880) Medical and biological imaging; (170.4940) Otolaryngology; (110.0113) Imaging through turbid media.

## References and links

1. H. Kubba, J. P. Pearson, and J. P. Birchall, "The aetiology of otitis media with effusion: a review," Clin. Otolaryngol. Allied Sciences **25**(3), 181–194 (2000).
2. M. Daniel, S. Imtiaz-Umer, N. Fergie, J. P. Birchall, and R. Bayston, "Bacterial involvement in otitis media with effusion," Int. J. Pediatr. Otorhi. **76**(10), 1416–1422 (2012).
3. C. Vertan, D. C. Gheorghe, and B. Ionescu, "Eardrum color content analysis in video-otoscopy images for the diagnosis support of pediatric otitis," in *10th International Symposium on Signals, Circuits and Systems* (IEEE, 2011), pp. 1–4.
4. L. Cheng, J. Liu, C. E. Roehm, and T. A. Valdez, "Enhanced video images for tympanic membrane characterization," in *2011 Annual International Conference of the IEEE Engineering in Medicine and Biology Society* (IEEE, 2011), pp. 4002–4005.
5. M. Sundberg, M. Peebo, Å. Öberg, P.-G. Lundquist, and T. Strömberg, "Diffuse reflectance spectroscopy of the human tympanic membrane in otitis media," Physiol. Meas. **25**(6), 1473–1483 (2004).
6. N. Bedard, I. Tošić, L. Meng, A. Hoberman, J. Kovačević, and K. Berkner, "In vivo middle ear imaging with a light field otoscope," in Optics in the Life Sciences, OSA Technical Digest (online) (Optical Society of America, 2015), paper BW3A.3.
7. N. H. Cho, S. H. Lee, W. Jung, J. H. Jang, and J. Kim, "Optical coherence tomography for the diagnosis and evaluation of human otitis media," J. Korean Med. Sci. **30**(3), 328–335 (2015).
8. R. Seth, C. M. Discolo, G. M. Palczewska, J. J. Lewandowski, and P. R. Krakovitz, "Ultrasound characterization of middle ear effusion," Am. J. Otolaryng. **34**(1), 44–50 (2013).
9. G. Fishman, A. DeRowe, E. Ophir, V. Scharf, A. Shabtai, D. Ophir, and A. Katzir, "Improved tympanic thermometer based on a fiber optic infrared radiometer and an otoscope and its use as a new diagnostic tool for acute otitis media," Proc. SPIE **3590**, 278–286 (1999).
10. P. Chandrasoma and C. R. Taylor, *Concise pathology* (Appleton & Lange, 1998).
11. K.-Z. Liu, A. Cholakis, M. G. Sowa, and X. Xiang, "Diagnosis and Monitoring of Gingivitis in vivo Using Non-Invasive Technology-Infrared Spectroscopy," in *Gingival Diseases - Their Aetiology, Prevention and Treatment*, F. Panagakos, ed. (INTECH Open Access Publisher, 2011).

#273691 http://dx.doi.org/10.1364/BOE.8.000230
Journal © 2017 Received 20 Sep 2016; revised 3 Nov 2016; accepted 4 Nov 2016; published 12 Dec 2016

Biomedical Optics EXPRESS

12. F. Leung, "Endoscopic reflectance spectrophotometry and visible light spectroscopy in clinical gastrointestinal studies," Digest. Dis. Sci. **53**(6), 1669–1677 (2008).
13. D. S. Jung, J. A. Crowe, J. P. Birchall, M. G. Somekh, and C. W. See, "Anti-confocal versus confocal assessment of the middle ear simulated by monte carlo methods," Biomed. Opt. Express **6**(10), 3820–3825 (2015).
14. D. Hidovic-Rowe and E. Claridge, "Modelling and validation of spectral reflectance for the colon," Phys. Med. Biol. **50**(6), 1071–1093 (2005).
15. D. Yudovsky and L. Pilon, "Rapid and accurate estimation of blood saturation, melanin content, and epidermis thickness from spectral diffuse reectance," Appl. Opt. **49**(10), 1707–1719 (2010).
16. M. Firbank, M. Oda, and D. T. Delpy, "An improved design for a stable and reproducible phantom material for use in near-infrared spectroscopy and imaging," Phys. Med. Biol. **40**(5), 955 (1995).
17. M. Firbank and D. T. Delpy, "A design for a stable and reproducible phantom for use in near infra-red imaging and spectroscopy," Phys. Med. Biol. **38**(6), 847 (1993).

## 1. Introduction

Otitis media with effusion (OME) is a chronic inflammatory disease that causes partial deafness. The air in the middle ear cleft is displaced by a mucin rich liquid. The viscosity of the effusion, caused by the mucin content, is too high to allow natural drainage of the middle ear via the Eustachian tube [1]. OME is a common disease in children and the only effective treatment is surgical drainage of the middle ear with insertion of a tympanostomy tube in the tympanic membrane done under general anaesthetic [2]. Tympanostomy tubes are spontaneously rejected by the eardrum on average after eight months, in 25 % of children the effusion recurs requiring further surgical treatment [2]. We hypothesise that the middle ear inflammation has not resolved in patients who have a recurrence of the effusion. Currently there is no clinically available method of measuring the inflammatory state of the middle ear mucosa. If there were, this would give clinicians a rational method of determining which patients need to be followed up and those which could be discharged from the clinic.

Several groups are working on a wide variety of novel diagnostic methods in order to improve the diagnosis of middle ear inflammation. Approaches include the use of image processing to enhance important features in otoscopic findings such as colour [3] or contrast [4], spectroscopic measurements [5], 3D shape extraction of the eardrum [6], 3D imaging techniques such as optical coherence tomography [7] and ultrasound [8], and temperature measurement [9]. While 3D imaging techniques reveal structures such as biofilms attached to the middle ear [7] or fluid inside the middle ear [8], they do not assess the inflammation of the mucosa itself. Spectroscopic methods and temperature measurement are better alternatives as they assess signs of inflammation itself via redness and a temperature increase, both signs of inflammation [10]. While the temperature signal is small and needs a reference measurement of a healthy ear [9], spectroscopic measurements are more promising even though the source (either eardrum or mucosa) of the measured signal cannot be determined and different cases of middle ear inflammation such as OME or acute otitis media can only be distinguished in statistical terms [5].

This project aims to improve the diagnosis of OME by predicting the recurrence after tympanostomy tubes extrusion. For this the inflammatory state of the middle ear mucosa needs to be assessed. We believe that spectroscopic measurement in the visible and near infrared range are most promising in diagnosing inflammation as they are already used in other fields of medicine such as diagnosing inflamed gums [11] and assessing blood flow in gastric mucosa [12]. However, spectroscopic methods cannot be used alone as signal components from the eardrum and the inflamed mucosa cannot be distinguished. Hence, our approach is to combine a spatial filtering method and spectroscopy in order to improve the diagnostic accuracy. In a previous paper [13] we introduced the anti-confocal system to allow multi-wavelength measurements through the eardrum while rejecting background signal from the eardrum. The system was simulated and its performance compared to the conventional confocal system showing superiority of the anti-confocal system for this measurement and its ability to detect signal from the mucosa while rejecting background from the eardrum.

Biomedical Optics EXPRESS

In this paper experiments will be conducted in order to confirm the simulations and assess the performance of the anti-confocal system when measuring inflammation on optical phantoms. This paper first describes the optical system and the optical middle ear phantoms used for tests of the system. Experimental results are described and interpreted afterwards.

## 2. Optical system

The principle of confocal detection is reversed in the anti-confocal system. Rather than detecting signal from a single point by use of a pinhole in the confocal case, the signal from a single point is rejected using a central stop instead. Using a larger diameter of the stop than is usual for a pinhole, the small point of rejection is increased to a volume of rejection, the higher the diameter the bigger the rejected volume. In case of measurements on the middle ear, this rejection volume as well as the focus of the illumination is placed on the eardrum and only signal from inside the middle ear is detected as shown in Fig. 1. A large area is sampled so decreasing the resolution but the signal level is increased compared to confocal detection. This allows easy sampling of a larger, more representative volume of the middle ear mucosa and assessment of the inflammation and is satisfactory as the aim is to detect and not image the inflammation.

The inflammatory state of the middle ear mucosa is linked to the metabolism of the tissue and thus its blood content. As blood is the main absorber in mucous tissues, an increased metabolism results in a higher absorption coefficient $\mu_a(\lambda)$ of the tissue and a decreased reflection signal $R$. When measuring the reflection signal of tissues in a wavelength range of high absorption (e.g. green), an increase of blood has a large influence on the signal. The effect is smaller in a wavelength region of generally smaller specific absorption of blood (e.g. NIR).

When direct measurement on a tissue is possible and no other parameters influence the measurement a single reflection signal can be used to measure the absorption and thus inflammatory state as the reflection is function of the absorption only $R = f(\mu_a(\lambda))$. In case of the middle ear, the eardrum obscures the view on the mucosa, attenuates and scatters the signal as well as adding background caused by reflections from the eardrum $R_{\text{eardrum}}$. Simplified, the signal can be described by

$$R(\lambda) = R_{\text{eardrum}}(\lambda) + R_{\text{mucosa}}(\mu_a(\lambda)) \cdot A(\lambda) \tag{1}$$

where $A$ is the attenuation of the eardrum. The anti-confocal system is used to minimise the background $R_{\text{eardrum}} \rightarrow 0$. Still, the attenuation $A$ of the eardrum is unknown. Using a two-wavelength measurement and the fraction of the signal at both measurements the attenuation factor can be reduced to one constant $c_A(\lambda_1, \lambda_2) = \frac{A(\lambda_1)}{A(\lambda_2)}$. We call this measure inflammation index $II$

$$II = \frac{R(\lambda_1)}{R(\lambda_2)} = \frac{R_{\text{eardrum}}(\lambda_1) + R_{\text{mucosa}}(\lambda_1) \cdot A(\lambda_1)}{R_{\text{eardrum}}(\lambda_2) + R_{\text{mucosa}}(\lambda_2) \cdot A(\lambda_2)} \approx \frac{R_{\text{mucosa}}(\lambda_1)}{R_{\text{mucosa}}(\lambda_2)} \cdot c_A(\lambda_1, \lambda_2) \tag{2}$$

If the attenuation at both wavelengths is similar $A(\lambda_1) \approx A(\lambda_2)$, the attenuation factor $c_A \approx 1$ can be neglected and the inflammation index directly measured. If this is not given, a way must be found to correct the inflammation index for changes in the attenuation at different wavelengths. Confocal detection of the eardrum parameters to do so is introduced later but for simplicity, a constant attenuation is assumed first. With an appropriate choice of wavelength, one in a high absorptive region and one in the low absorptive region of haemoglobin the dependence of this index on the blood content and thus inflammation can be maximised. A good choice is a NIR laser for $\lambda_1$ and a green laser for $\lambda_2$.

The setup of the optical system is illustrated in Fig. 1. Two lasers (532 nm: BWN-532-30, B&W Tek, Newark, DE, USA and 808 nm: L808P010 controlled by the power and temperature controller kit LTC100-B LD, Thorlabs, Newton, New Jersey, USA) are aligned, combined, and their beam expanded to a radius of 6 mm. The beam is directed on the middle ear by a beamsplitter and is focused by a lens with focal length $f = 80$ mm resulting in a NA of 0.08

Biomedical Optics EXPRESS

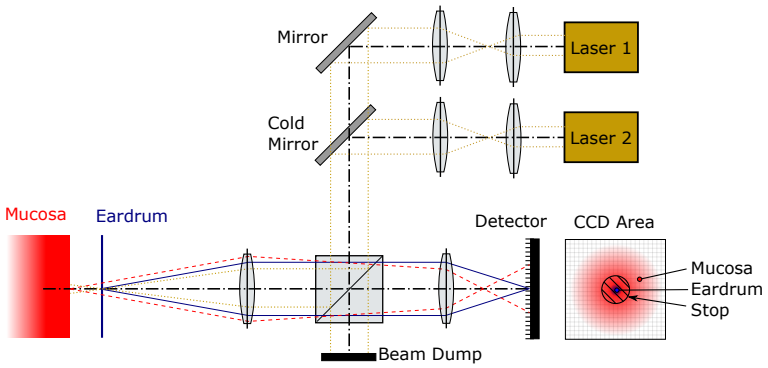


Fig. 1. Optical system consisting of beam expansion and alignment of two lasers and the anti-confocal setup including beam splitter, focusing lenses, and CCD detector allowing filtering in post-processing. Illumination is shown in yellow, background from the eardrum in blue, and signal from the mucosa in red. The expected signal distribution on the CCD is also shown.

(maximum possible in the ear). The eardrum is in focus and the mucosa is placed 4 mm behind the eardrum as it is the case in the human ear. The reflected signal from the eardrum is focused on a CCD camera (iXon EM+, Andor, Belfast, Northern Ireland) with 14 bit resolution, while the signal from the mucosa is out of focus.

Next to the optical setup, the area of the CCD is illustrated and the distribution of the beams schematically shown. The signal from the eardrum (blue) is in focus and centred in the middle of the camera while the signal from the mucosa (red) is wider spread. Anti-confocal filtering is done in software by selecting only pixels outside the black circle indicating the stop. Choosing a large enough diameter of the stop, the signal from the eardrum is rejected. The radius of the stop is easily altered in software and allows closer investigation of the signal than would be the case when using a physical stop.

## 3. Middle ear phantom

Experiments are conducted on a middle ear phantom composed of eardrum and mucosa. Four different phantoms were created for the mucosa, matching its optical properties (scattering and absorption) of healthy and inflamed tissue, and two intermediate cases.

The absorption coefficient is modelled similar to [14]

$$\mu_a(\lambda) = \frac{V_{Hb}\ln(10)c_{Hb}\cdot(\alpha\epsilon_{HbO2}(\lambda)+(1-\alpha)\epsilon_{Hb}(\lambda))}{64500\ [g/mol]} \tag{3}$$

where $V_{Hb}$ is the blood volume fraction, $\epsilon_{HbO2}$ is the molar extinction of oxy-haemoglobin, $\epsilon_{Hb}$ the molar extinction of haemoglobin, $\alpha$ the oxygenation of the blood, and $c_{Hb} = 120$ g/l the concentration of haemoglobin per litre of blood. The absorption is scaled according to

$$\mu_{a,scaled} = 0.62\cdot\mu_a + 0.03 \tag{4}$$

in order to match average tissue properties found in a wide literature search. Linear scaling was chosen as the offset introduces tissue background absorption, as proposed by Yudovsky [15]. The scattering anisotropy of the phantoms is about 0.5 [17] while it is around 0.9 for tissue. Hence, the scattering characteristics cannot be easily reproduced. Monte Carlo simulations were conducted to find a scattering coefficient of the phantoms approximating the reflection characteristics of mucosa. This results in the reduced scattering coefficient of 6 $mm^{-1}$ at 808 nm. Only the blood

Biomedical Optics EXPRESS

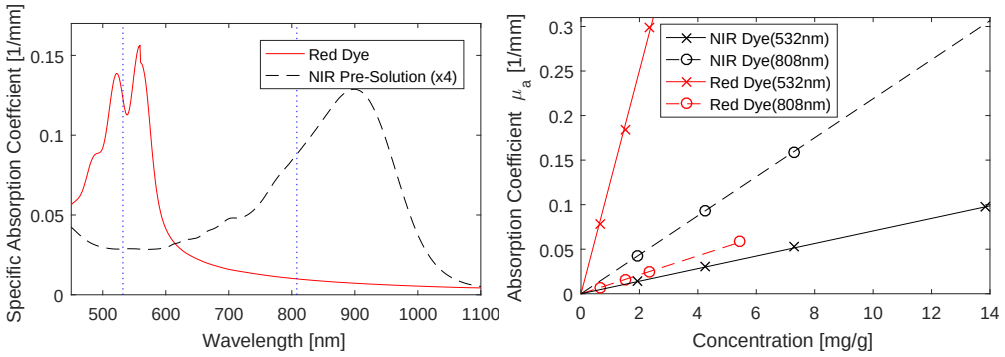


Fig. 2. Characterisation of the dyes. Spectrum of both dyes on the left and absorption coefficient at two wavelengths dependent on dye concentrations on the right.

concentration is varied in the different phantoms, while scattering and oxygenation are kept constant as no clear change of these properties is reported in literature.

To create the optical phantoms a recipe provided by the Biomedical Optics Research Laboratory, UCL, is adopted. A clear polyester resin (405-210, Tiranti Ltd., Thatcham, UK) mixed with a Liquid Hardener (405-810, Tiranti Ltd. Thatcham, UK) is used as base material. The $TiO_2$ based colour Superwhite (407-220, Tiranti Ltd. Thatcham, UK) introduces scattering and the dye ProJet 900NP (Fujifilm, Minato, Tokyo, Japan) introduces absorption [16]. The dye "Polyester Pigment: Translucent Red" (407-330, Tiranti Ltd. Thatcham, UK) was added to the recipe in order to match optical properties at two wavelengths. This dye does not add scattering to the phantom as characterised in experiments.

The absorption spectra of both dyes diluted in the polyester resin without scattering medium or hardener added were characterised using a spectrometer (Libra S32PC, Biochrom, Cambridge, UK) and the results are shown in Fig. 2(a). Four mixtures with different concentrations $c$ were measured in order to characterise the dependence of dye concentration and absorption coefficient. The relation is shown in Fig. 2(b) for both dyes at the two laser wavelengths. Instead of using the NIR dye directly, a pre-solution (1:100, dye:resin) was used for easier mixing of the materials.

The absorption coefficient of a phantom is determined by

$$\mu_a(\lambda) = c_{red} \cdot \alpha_{red}(\lambda) + c_{NIR} \cdot \alpha_{NIR}(\lambda) \tag{5}$$

with the specific absorption coefficient of the dye $\alpha_{red}(808) = 0.010\,mm^{-1}$, $\alpha_{NIR}(808) = 0.022\,mm^{-1}$, $\alpha_{red}(532) = 0.123\,mm^{-1}$, and $\alpha_{NIR}(532) = 0.007\,mm^{-1}$ and the concentration given in mg/g (dye/resin).

Blood volume fractions $V_{Hb}$ of 2, 8, 14, and 20 % (within the range of concentrations possible in mucous tissues [14]) were chosen for the mucosa phantoms. The absorption of the red dye is too high at 808 nm resulting in a theoretical negative concentration of the NIR dye. Hence, the desired absorption at 808 nm is slightly increased resulting in the final properties of the phantoms as given in Tab. 1.

As the scattering angle of the eardrum cannot be easily reproduced using the above recipe giving a fixed scattering anisotropy, different methods to create an eardrum phantom are investigated. These include the use of tracing paper, an optical diffuser, with sandpaper treated glass slides, and fibre glass mats cast in resin. Tracing paper shows much higher scattering than eardrums. The properties of fibre based phantoms and sanded glass slides are hard to control and result in inhomogeneous samples. Thus, the 1500 grid ground glass diffuser (DG20-1500, Thorlabs, Newton, New Jersey, USA) is used as eardrum phantom for further characterisation. The diffuser shows higher scattering than expected for the eardrum ($\mu_{s,diffuser} = 40\,mm^{-1}$ compared

Biomedical Optics EXPRESS

Table 1. Desired optical coefficients and required concentrations of scattering and absorbing agents for the mucosa phantoms.

| Phantom | $V_{Hb}$ [%] | $\mu_s'(808)$ [mm$^{-1}$] | $c_{scat}$ [g/kg] | $\mu_a(532)$ [mm$^{-1}$] | $\mu_a(808)$ [mm$^{-1}$] | $c_{red}$ [g/kg] | $c_{NIR}$ [g/kg] |
|---|---|---|---|---|---|---|---|
| 1 - Healthy | 2 | 6 | 7.5 | 0.244 | 0.173 | 1.571 | 7.131 |
| 2 - Intermediate 1 | 8 | 6 | 7.5 | 0.873 | 0.173 | 6.832 | 4.754 |
| 3 - Intermediate 2 | 14 | 6 | 7.5 | 1.502 | 0.173 | 12.093 | 2.377 |
| 4 - Diseased | 20 | 6 | 7.5 | 2.131 | 0.173 | 17.354 | 0 |

to $\mu_{s,eardrum} = 11\,\text{mm}^{-1}$ as best matches of Monte Carlo simulations and measurements; with scattering anisotropy $g = 0.99$ and negligible absorption compared to the scattering coefficient) resulting in increased attenuation of the signal and can be seen as a worst case eardrum phantom.

## 4. Experimental results

### 4.1. Axial sectioning

The sectioning capability of the anti-confocal system is measured by scanning a mirror along the optical axis and recording the detected signal power. Figure 3 shows the results without filtering (0 µm stop radius), 240, 480, and 720 µm stop radius. The theoretical detected power, calculated by geometrical optics, is shown as well. The mirror is in focus at $z = 0$ (where the eardrum would be placed) and moving away from the optical system with increasing $z$. Around $z = 0$, the stop rejects the reflections from the mirror resulting in lowest signal and background components of an eardrum placed here will be rejected as observed later. An increasing stop radius increases the range on the optical axis where signals are rejected. The decreasing power observed in measurements and theory at positions $z > 0$ is a result of light reflected outside the detection NA due to the increased distance of optics to the scanned mirror.

### 4.2. Measurement of the inflammation index

Next, the reflected power from the four mucosa phantoms with the diffuser placed in the beam path as well as the signal from the diffuser only is measured for both wavelengths and the detected power per radius from the optical axis shown in Fig. 4.

The highest power is observed in the center where the signal from the eardrum is focused. In this area, the signal from the different phantoms cannot be distinguished for the same measure-

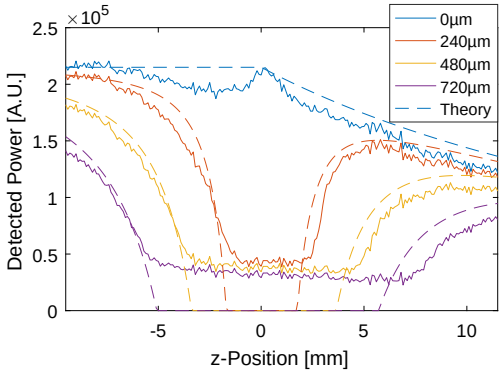


Fig. 3. Signal detected by an anti-confocal system with stop radius according to the legend, when scanning a mirror along the optical ($z$) axis.

Biomedical Optics EXPRESS

ment wavelength. Only at a higher radii do the signals differ, the signal from the eardrum phantom falls off quickly and also a difference in the signal from the mucosa phantoms becomes visible. The NIR signal is generally higher than the green signal and the green signal decreases from phantom 1 to 4 while the NIR signal increases. This is a result of the wavelength depended absorption coefficient of the mucosa phantoms, increasing from phantom 1 to 4 in the green range and decreasing in the NIR range.

During signal processing the central pixel of the camera are not used for evaluation forming a virtual stop to reject the signal from the eardrum. The rest of the power is summed to calculate the total reflected signal. Figure 5 shows the total reflected signal as solid lines and signal when using stop filtering with different radii as dashed lines for all four phantoms in the sample plot. Instead of the mucosa phantom number, their absorption coefficient at 532 nm is given on the x-axis. The left figure shows the green while the right figure shows the NIR signal. All plots are normalised to their respective maximum value to allow easy comparison of the graphs that would otherwise show decreasing signal levels with increasing stop radius. 5 measurements were taken for each phantom, the mean is shown here and the errorbars indicate the standard deviation.

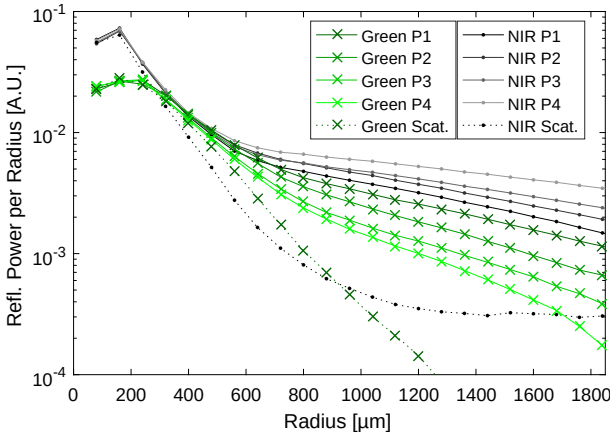


Fig. 4. Distribution of the detected power plotted over radius from center of the camera. The measurement was taken on five phantoms; mucosa phantom 1 to 4 with eardrum phantom placed in front (P1–4) and eardrum phantom only (Scat.), each measured at both wavelengths, green and NIR.

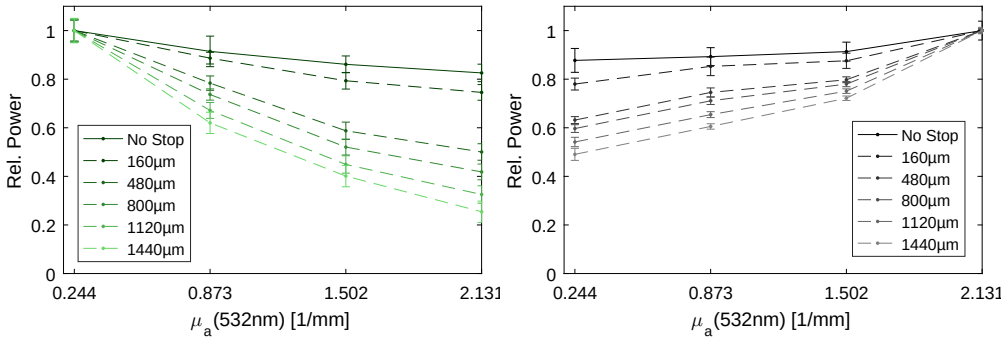


Fig. 5. Detected power with varied stop radius, according tot legend, as a function of the mucosa phantom absorption coefficient. An increase on the x-axis denotes increasing blood level and thus inflammation. Error bars indicate the standard deviation of five measurements. Measured at 532 nm on the left and 808 nm on the right.

Biomedical Optics EXPRESS

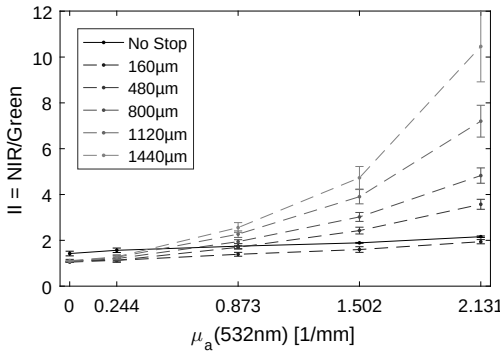


Fig. 6. Inflammation index for different stop radii, according to legend, as a function of $\mu_a$. Again, an increase on the x-axis denotes increasing inflammation.

The green signal is highest for phantom 1 and lowest for phantom 4 in contrast to the NIR signal which increases. The contrast between the detected power from each phantom increases with increasing stop radius.

In the next step, the earlier introduced inflammation index $II = \frac{R(808)}{R(532)}$ is calculated and results shown in Fig. 6 for different stop radii in dependence on the absorption of the phantoms at 532 nm. Additionally to the four mucosa phantoms a white phantom without attenuation is included in the graph. Again the mean of 5 measurements is shown and the standard deviation shown as errorbars. All plots show an increase of the index with increasing modelled blood content of the phantoms. Similar to the reflected power, the difference in index increases with stop radius. But the standard deviation increases at the same time. The ideal index would have a linear and high slope while keeping the variation small. Hence, the measure $M$ for a good index is defined as

$$M = \frac{m \cdot R^2}{\sigma} \tag{6}$$

where $m$ is the slope of a linear interpolation of the index $II = m * \mu_a + b$, $R^2$ is the coefficient of determination indicating the goodness of the linear fit, and $\sigma$ is the average standard deviation of the 5 measurements. In the shown example this results in a best inflammation index when using a stop radius of 640 µm. Averaging the best stop radius over all measurements for different variations of the phantom as presented below results in a stop radius of 576 µm.

### 4.3. Variation of the middle ear phantom

The dependence of the inflammation index on phantom parameters is tested and results shown in Fig. 7, where markers show the measured values and the lines are linear fits for each series. For the curve “Standard”, the diffuser was used as eardrum phantom, the distance between eardrum and mucosa was 4 mm and the angle between optical axis and the surface normal 10 °. The index was measured three times, the average is shown and the errorbars indicate the standard deviation. In the variation cases only one parameter is changed each. Results for changed scattering scattering of the eardrum, angle between phantoms surface and optical axis, and distance between eardrum and mucosa are shown in subfigure (a), while subfigure (b) shows the change due to absorption of the eardrum.

**Distance** between eardrum and mucosa: The distance was varied from 2 to 6 mm with the 2 mm case shown. A decreasing distance results in an increase of the measured index.

**Angle** between optical axis and normal of sample surface: The angle is varied from 0 to 10 ° (0 ° shown) and a decrease in angle results in a decrease of the inflammation index (difference

Biomedical Optics EXPRESS

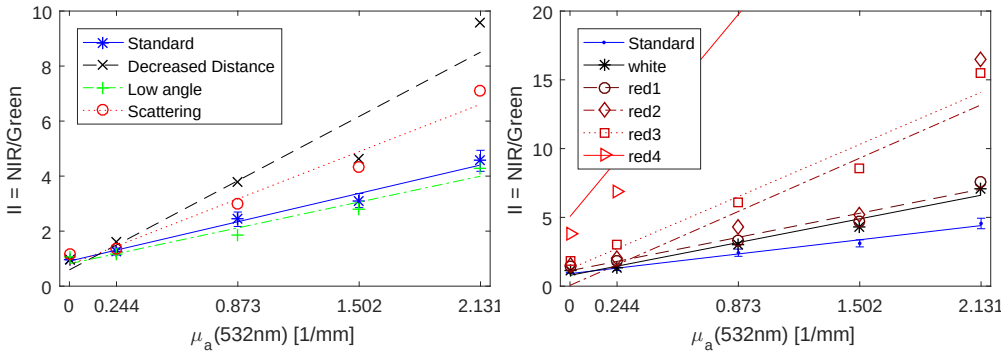


Fig. 7. Inflammation index dependent of variations of the sample. A stop radius of 576 µm is used. The left figure shows the influence of angle, distance, and scattering of the eardrum while the right figure shows the influence of absorption of the eardrum on the measured inflammation index. Measurements are shown as nodes and linearly interpolated.

is more visible for smaller stop radii than shown here).

**Scattering** of the eardrum: The diffuser was replaced by other phantoms such microscope slides whose surface is roughened with sand paper, and fibre glass cast in resin (shown here). A change in scattering can have an influence on the measured index as shown here while other samples do not.

**Absorption** of the eardrum: The absorption of the fibre glass sample was altered by adding dye to the resin. Red dye with increasing concentration from sample 1 to 4 was added. The wavelength dependent absorption of the eardrum strongly affects the measured index.

### *4.4. Confocal detection of eardrum properties*

As a camera is used as the detector and the optical system focused on the eardrum, confocal detection can be easily used to sample the eardrum. This could give information about its properties and help to correct the measured inflammation index for changes in absorption and scattering. The coloured fibre glass samples used to change the absorption of the eardrum phantom are used to test whether it is possible to correct the inflammation index for changes of absorption of the eardrum.

The confocal signal is measured for the four eardrum phantoms and the relation of detected power of NIR to green $s_{\text{confocal}}$ shown in Fig. 8(a), with the x-axis scaled according to the red dye concentration in each eardrum phantom. The confocal signal was measured 6 times (each time the mucosa phantom was changed), the average,standard deviation, and linear interpolation are shown. The confocal signal is dependent on the attenuation of the eardrum as expected and will be used for correction of the inflammation index $II$. To do so, the scaling factor must be calibrated. For this, first the slopes of the measured inflammation indices $m_{\text{II}}$ is calculated for a linear approximation

$$II = m_{\text{II}} \cdot \mu_{\text{a}}(532) + b \tag{7}$$

The inverse of this slope $\frac{1}{m_{\text{II}}}$ scales the different indices correctly, but obviously, is not available in later measurements. Hence, the relation between the confocal signal and the needed scaling factor $c = \frac{1}{m_{\text{II}}}$ must be found. Again, a linear interpolation is used.

$$c = \frac{1}{m_{\text{II}}} = m \cdot s_{\text{confocal}} + b \tag{8}$$

Biomedical Optics EXPRESS

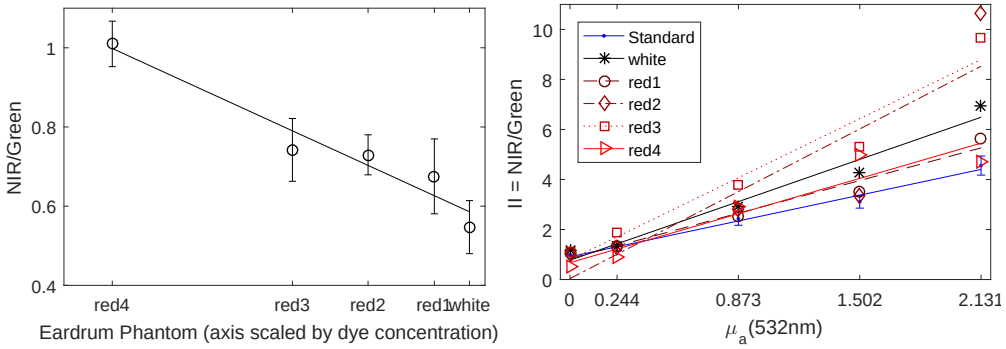


Fig. 8. Correcting the inflammation index. The left figure shows the relation of the confocal signal measured at 808 and 532 nm for each eardrum phantom, with the error bars indicating the standard deviation of six measurements and measurements linearly interpolated. The right figure shows the corrected inflammation index for each eardrum phantom in dependence on $\mu_a$, increasing with worsened inflammation along the x-axis. The measurements are indicated by the nodes and linearly interpolated.

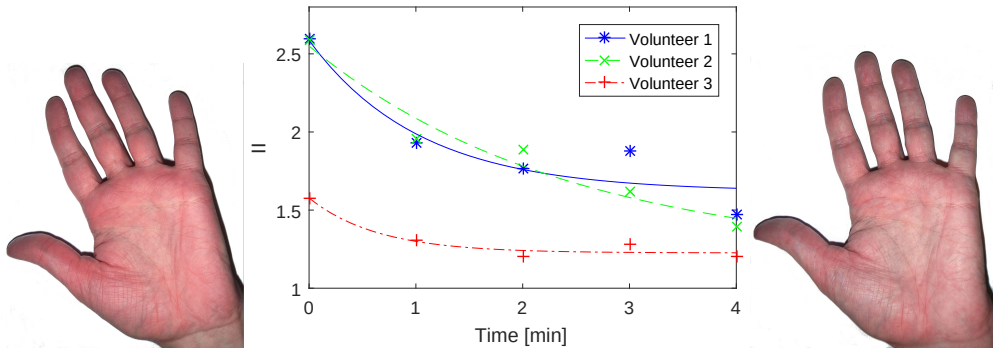


Fig. 9. Time course of the inflammation index measured on human volunteers. The photographs show the hand of volunteer 2 before ($t = 0$) and after ($t = 4$) the measurement series. The measurements are exponentially interpolated.

Figure 8(b) finally shows the measured inflammation index corrected by $c$ and clearly shows an improvement to the unscaled signal shown in Fig. 7(b). The test and calibration data are the same. Further, no scattering is included into this model.

### 4.5. Test on real blood circulation

To verify the model for absorption of blood in tissue, experiments were conducted on the hands of human volunteers. Three volunteers were asked to submerge their hand in cold water (about 5 °C) for 5 minutes; this increases the blood volume in the hand in order to raise the temperature of the hand. The inflammation index of the hand was then measured through an eardrum phantom over 4 minutes with the measurements shown in Fig. 9(b). The markers indicate measurements and the lines are exponential interpolations $II_{\text{fit}} = a \cdot \exp(b \cdot t) + c$ with the $R^2$ values of 0.890, 0.957, and 0.947. Subfigure (a) and (c) show photographs of the hand before and after the measurement series. The inflammation index decreases from $t = 0$ measured directly after the hand was removed from the water to $t = 4$ minutes later. Different absolute values are measured but the course of all curves is similar and shows a decrease over time.

Biomedical Optics EXPRESS

## 5. Discussion

### 5.1. Axial sectioning

Measurements and theory of the axial sectioning of the anti-confocal system fit well and show that a stop with increasing radius blocks more signal, reducing the detected power and increasing the range on the optical axis where unwanted signal components are rejected. The fluctuations in the measurements stem from variations in the background level of the camera, amplified by summation of a large area and small signal components. Drifts of the background level over time result in an offset causing the signal not to reach zero when blocked by the stop at $z$ around 0, in contrast to theory. This problem is solved in the other experiments presented in this paper by repeated background level measurements, which were not done during the z-scan performed here.

### 5.2. Measurement of the inflammation index

The optical mucosa phantoms were designed to have a constant absorption coefficient in the NIR range. This is not the case as the measured signals show. The absorption decreases from phantom 1 to 4, indicated by an increase of the detected reflection signal. This is caused by errors of the spectral characterisation of the dyes. The absorption at 808 nm measured here is lower compared to the data given in [16]. This causes small errors in the recipe resulting in optical properties of the created mucosa phantoms that differ from the desired values. This increases the measured inflammation index and the contrast between the phantoms. Nonetheless these phantoms were used instead of creating a new set of more accurate phantoms as the change in absorption in the green range constitutes most to the measured inflammation index and the error in absorption coefficient does not influence the measurement significantly. Despite this error and approximations of the model, the middle ear phantom is accurate enough to characterise the anti-confocal system and simulate the human ear because the human ear shows variations and hence exact properties of the phantom are not necessary and second the change in blood content is still approximated by the four different mucosa phantoms.

The radial power distribution in Fig. 4 is maximal the center as the reflections from the eardrum are focused on the camera. The signal falls off with increasing radius from the center as first no directly reflected but only scattered signal reaches the detector and the scattered signal then decreases as more signal is absorbed when propagating further from the illuminated area. The center shows a higher power for NIR radiation because the surface roughness is close to the wavelengths used and hence the reflection characteristics are wavelength dependent. This also causes the green reflections to show a wider scattering angle than the NIR reflections. The difference of the signals recorded from the different mucosa phantoms at higher radii is easily explained by the absorption coefficient of the phantoms. The signal decreases from phantom 1 to 4 in the green range while the opposite is true for the NIR range, according to the absorption coefficient.

The anti-confocal stop is effective in removing the background from the eardrum as this component is centred close to the optical axis. Further, the defined inflammation index is sensitive to changes in the simulated blood concentration in the phantoms. The contrast in detected power and slope of the inflammation index increases with increasing stop radius because the background due to reflections from the eardrum is blocked first and then photons with a shorter pathlength in the mucosa phantom are blocked. Photons with a longer pathlength are more effected by the absorption than phantoms with a short pathlength and hence, the contrast increases when only detecting photons with long pathlength carrying more information about the absorption coefficient. But at the same time, the signal level is reduced, increasing the influence of noise which is shown by the increased standard deviation when using stops with higher radii. An optimum stop radius results in a trade-off between low noise and high contrast and

Biomedical Optics EXPRESS

is dependent on the optical properties of the sample as well as the detector properties such as dynamic range and detector noise determining the lowest detectable signal level. A measure for a best stop radius was defined, finding the best compromise at a radius of 576 µm for the current set-up and optical properties of interest. This value was used in the presented experiments.

The specifications of the anti-confocal system, such as background rejection ratio and sampled area cannot be generalised and depend on the optical properties of the sample, stop size, and detector.

### 5.3. Variations of the middle ear phantom

The experimental results show that the inflammation index is distorted by different parameters of the sample. An increased distance between eardrum and mucosa causes the illuminated area on the mucosa to increase according to the scattering characteristics and NA of the illumination beam as the light is focused on the eardrum. This causes more power to be detected off axis and increases the signal as the stop rejects only signals close to the optical axis. Compared to the NIR signal, the green signal is generally lower and has a smaller pathlength due to a higher absorption coefficient. An increase of the illuminated area thus has a larger effect on the green signal and consequently reduces the measured inflammation index.

The measured inflammation index increases with the angle between the optical axis and surface normal of the sample as direct reflections are directed away from the optics and the background power is reduced even without applying a stop.

Both scattering and absorption characteristics of the eardrum also affect the inflammation index, especially in cases where these changes are wavelength dependent. The eardrum phantom with changed absorption attenuates the green light stronger than the NIR. As the light passes the eardrum twice, the effect of absorption is squared and the strong increase on the inflammation index is explained. A wavelength dependent as well as a wavelength independent change in scattering affects the inflammation index. Both signal power and signal distribution are altered affecting the index.

While the anti-confocal system is effective in rejecting background signals from the eardrum this section shows that it is not able to account for changes in properties of the middle ear affecting measurement of the inflammation index.

### 5.4. Confocal detection of eardrum properties

To account for changes in the eardrum, confocal detection of its parameters was introduced. The confocal detected reflectance of the glass fibre eardrum phantoms shows a dependence on the absorption determined by the dye concentration. This was used to correct the inflammation index and yield improved results. But as the resolution of the confocal system is low $r_{\mathrm{axial}} = 1.5n\frac{\lambda}{NA^2} \approx 188\,\mu\mathrm{m}$ at 808 nm, also reflections from the eardrum surface are detected. This results in the high variation of the confocal signal and will reduce the improvement by correction when done on a different data set.

While confocal detection of the eardrum properties accounts for changes of the absorption of the eardrum, it cannot account for changes in scattering or other properties of the middle ear.

### 5.5. Test on real blood circulation

The measured inflammation index of the hands shows the expected course, it is highest in the beginning when the blood volume is highest in the hand. This is established by the red appearance of the hand in the photograph. The measured index decreases over time as the blood volume decreases and the colour of the skin goes back to normal as seen in the second photograph. The difference of absolute values between the volunteers result from differences in the skin thickness, perfusion, and response to exposure to a cold environment.

Biomedical Optics EXPRESS

This experiment shows that the blood level of living tissue can be measured through an eardrum phantom and measurements will also be possible in the ear as the described measurements were performed through the thick skin on the human palm, not present and disturbing measurements in the ear. Also, the correctness of the mucosa phantoms is confirmed.

## 6. Conclusion

The anti-confocal system was shown to be able to reject background signals while still detecting information about the inflammation when measured through a scattering layer approximating the eardrum properties. The severity of the inflammation is assessed via the blood content of tissue, simulated by polyester resin based mucosa phantoms and human hands exposed to cold, and measured by the in this paper defined inflammation index.

This modelled inflammation can be assessed in all investigated middle ear phantoms but the index is distorted by other parameters of the middle ear such as scattering and absorption of the eardrum or size of the middle ear cavity. This means, the index is subject to sample variations not connected to the inflammation itself. This makes measurements of the inflammation index challenging in humans with where properties of the middle ear vary. A way to improve the measurements is the use of the confocal signal from the eardrum (detected in parallel to the anti-confocal signal) to determine its properties and use this information to correct the index. But the current signal processing model does only account for absorption of the eardrum but not for other changes in the middle ear.

We believe the presented method is promising because information about the inflammation could be extracted in all measurements. The remaining problem is the influence of other parameters in the middle ear, such as colour and translucency of the eardrum, distorting the measurements. While we introduced a method to correct for some of these effects, further refinement of the signal processing may be necessary to overcome all influences and ensure repeatable measurements. We believe that more sophisticated correcting techniques can be implemented making use of the pixelated nature of the detector. Once this is achieved, the system can enter clinical trials. We believe, that in addition to improved signal processing, experimental calibration of the system on many subjects will be necessary to overcome the problem of the wide variety of properties encountered in different patients. Similar calibration techniques are used in other spectrophotometry based techniques such as oximetry and have been shown to achieve acceptable accuracy for clinical use.

## Funding

National Institute for Health Research (501100000272).

## Acknowledgments

This report is independent research part funded by the National Institute for Health Research Biomedical Research Unit Funding Scheme. The views expressed in this publication are those of the authors and not necessarily those of the NHS, the National Institute for Health Research or the Department of Health.

We thank Prof. Jeremy Hebden, Biomedical Optics Research Laboratory, UCL, for providing the original recipe and instructions to create the tissue phantoms.